Atomic scale determination of surface facets in gold nanorods.

Bart Goris [1], Sara Bals [1,*], Wouter Van den Broek [1,3], Enrique Carbó-Argibay [2], Sergio Gómez-Graña [2], Luis M. Liz-Marzán [2], Gustaaf Van Tendeloo [1]

1 Electron Microscopy for Materials Research (EMAT), University of Antwerp, Groenenborgerlaan 171, 2020 Antwerp, Belgium.

2 Departamento de Química Física, Universidade de Vigo, 36310 Vigo, Spain

3. Institute for Experimental Physics, Ulm University, Albert-Einstein-Allee 11, 89081 Ulm, Germany

Nature Materials 11, 930–935 (2012) doi:10.1038/nmat3462

* sara.bals@ua.ac.be

It is widely accepted that the physical properties of nanostructures depend on the type of surface facets[1,2]. For Au nanorods, the surface facets have a major influence on crucial effects such as reactivity and ligand adsorption and there has been controversy regarding facet indexing[3,4]. Aberration corrected electron microscopy is the ideal technique to study the atomic structure of nanomaterials[5,6]. However, these images correspond to two-dimensional (2D) projections of three-dimensional (3D) nano-objects, leading to an incomplete characterization. Recently, much progress was achieved in the field of atomic resolution electron tomography, but it is still far from being a routinely used technique. Here we propose a novel methodology to measure the 3D atomic structure of free-standing nanoparticles, which we apply to characterize the surface facets of Au nanorods. This methodology is applicable to a broad range of nanocrystals, leading to unique insights concerning the connection between structure and properties of nanostructures.

A thorough understanding on the atomic structure of free-standing nanocrystals and the formation of facets at their surface is required to optimize their properties. For Au nanocrystals, it is known that the catalytic and optical properties can be tuned in a reproducible manner by controlling their morphology[7,8]. Surface morphologies of nanocrystals can be characterized in 3D using electron tomography[9-11], but often the resolution is insufficient to allow a straightforward characterization of the crystallographic planes at the surface. Significant progress, pushing the resolution in 3D to the atomic level, has recently been achieved[12-14]. Based on a limited number of high angle annular dark field scanning transmission electron microscopy (HAADF-STEM) images, a 3D reconstruction at the atomic scale could be obtained for a Ag nanoparticle with a diameter of approximately 3 nm, which was embedded in an Al matrix. These results were obtained using advanced statistical parameter estimation and so-called discrete tomography[12]. This approach is currently based on the assumption that all atom positions are fixed on a grid and this has been shown to be a good starting point to obtain unique insights concerning the formation of nanoparticles. However, for larger particles it becomes more

challenging or impossible to count the atoms in a column in a straightforward manner. Therefore other approaches should be explored. The use of prior knowledge in such 3D reconstruction techniques should be avoided in order to enable an unbiased and direct indexation of the surface facets. Recently, Scott et al. reported the atomic scale reconstruction of a distorted icosahedral multiply twinned Au nanoparticle with a diameter of ~10nm[14]. Although not all atoms could be located in this reconstruction, valuable information concerning lattice parameters and grains inside the particle could be obtained. It must be noted however that 55 images were required to obtain this 3D reconstruction.

Here, we propose a compressive sensing based 3D reconstruction algorithm, which enables us to completely characterize the 3D atomic lattice of free-standing Au nanorods. Based on a limited number of HAADF-STEM projection images, a high quality 3D reconstruction of the atomic structure is obtained without the use of any prior knowledge. From the final reconstruction, the surface facets of the rods can be characterized with a high precision. In addition, imperfections at the atomic scale and surface relaxation is studied. We applied our approach to Au nanorods which have important applications in the field of nanoplasmonics, but the methodology is applicable to a wide variety of nanostructures.

Because of their well-defined anisotropy and the interaction between shape and optical response, Au nanorods have been studied extensively[3,4,15]. We investigated Au nanorods, obtained by seed-mediated growth in aqueous solution, assisted by the surfactant cetyltrimethylammonium bromide (CTAB) and Ag^+ ions[16]. In addition, since Au nanorods prepared by seeded growth in the presence of a gemini surfactant were recently used for the analysis of nanorod crystallography[3], we also studied these for comparison. More details concerning the synthesis procedure can be found in the methodology section. Electron tomography at relatively low magnification in combination with electron diffraction was used to determine the overall morphology of the rods. The details of this procedure are discussed in the methodology section. The results are presented in figures 1a and 1b, revealing a facetted morphology for both type of rods, in agreement with previous reports[3,4,17]. However, the resolution that can be obtained at this magnification prevents a correct indexing of the side facets of these reconstructions.

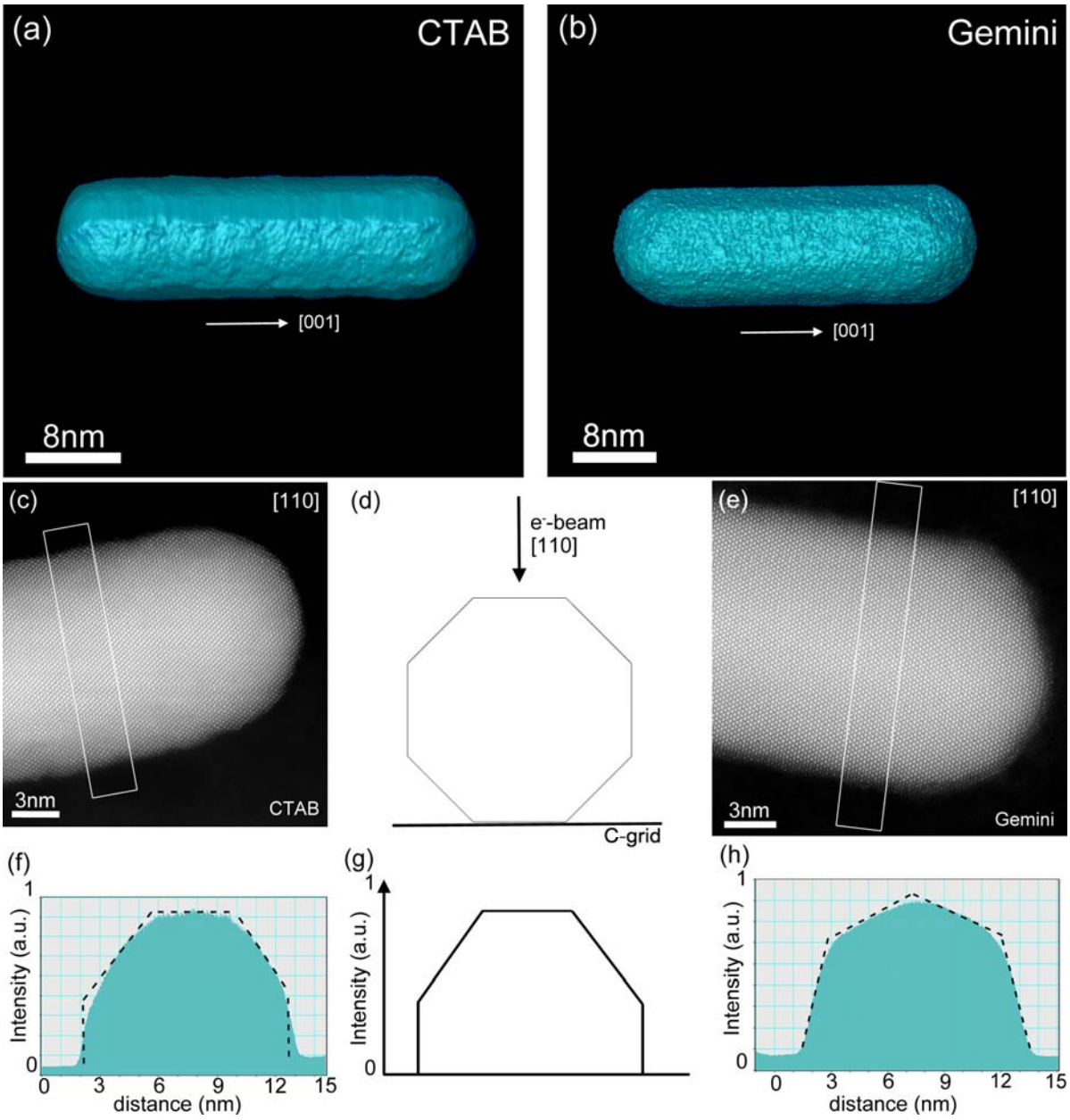

Figure 1: Comparison between Au nanorods grown with CTAB and Gemini surfactants. (a and b) 3D visualizations of tomographic reconstructions of both types of nanorods. Crystal facets are visible in both tomographic reconstructions. (c-e) High resolution HAADF-STEM projection of both nanorods oriented along the [110] direction. The intensity profile acquired from the first projection (f) corresponds to a model where the morphology is composed of {110} and {100} facets (d and g). The intensity profile acquired from the projection of the rod grown with the Gemini surfactant (h) clearly shows a deviation from this model.

These observations are complemented by intensity profiles acquired from high resolution HAADF-STEM images. HAADF-STEM yields a signal that is proportional to the thickness of the specimen and to the atomic mass of the atoms in the sample[18-20]. In this case, the HAADF-STEM intensity therefore corresponds to a thickness profile of the Au nanorods. For both types of nanorods, a HAADF-STEM image is acquired along a [110] zone axis as shown in figures 1c and 1e. The intensity profile acquired along the direction perpendicular to the major axis is displayed in figures 1f and 1h. These results suggest that the morphology of the rod grown with CTAB is mainly composed of {110} and {100} facets as illustrated by the correspondence with the model in figures 1d and 1g, in agreement with early characterization[17]. This analysis also indicates that the morphology of the rods grown with the Gemini surfactant deviates from this model structure, as recently reported[3].

The analysis described above presents a first step towards the full 3D characterization of the morphology of the nanorods. Next, 4 different high resolution HAADF-STEM images were acquired along different zone axes ([100], [110], [010] and [$\bar{1}$10]) for nanorods prepared using the CTAB surfactant and nanorods grown with the Gemini surfactant. After alignment of the images, they are used as an input for a novel tomographic reconstruction algorithm based on compressive sensing (CS)[21,22]. Compressive sensing is a technique specialized in finding a solution that has a sparse representation to a set of linear equations. Recently, the advantages of using compressive sensing for electron tomography were demonstrated for reconstructions with nanoscale resolution[23,24]. For 3D reconstructions at the atomic scale, it is valid to exploit the sparsity of the object (and its 3D reconstruction) since only a limited number of voxels contain an atom and most voxels correspond to vacuum. Using this prior knowledge in a tomographic reconstruction algorithm will result in a more reliable atomic scale reconstruction as compared to more conventional reconstruction algorithms such as the simultaneous iterative reconstruction technique (SIRT)[25]. Another advantage is that because of the sparsity incorporated in the reconstruction algorithm, a very limited number of projections are sufficient to create a faithful reconstruction of the atomic lattice. It should be noted that although we assume the object to be sparse, no assumptions are made concerning the position of the atoms.

In a conventional SIRT algorithm, one starts with a first 3D reconstruction that is re-projected along the directions of the original acquisition angles. The difference between the (2D) re-projections and the original (2D) projections is called the projection error. When using SIRT, this projection error is iteratively minimized by adding the reconstructed projection error to the previous intermediate reconstruction. Mathematically, a tomographic reconstruction corresponds to reconstructing an object x starting from its projections b, which are acquired by a projection operator A. The tomographic reconstruction then often corresponds to iteratively solving the following minimization problem.

$$\hat{x} = \arg\min_x \|Ax - b\|_2^2$$

In the CS algorithm employed in this work, an additional penalty parameter λ is introduced leading to a simultaneous minimization of the projection error and the L1-norm of the object (i.e. the sum of the absolute values of all the voxels in the reconstructed object)[26]:

$$\hat{x} = \arg\min_x \left[\|Ax - b\|_2^2 + \lambda \|x\|_1 \right]$$

The reliability of the reconstruction algorithm is confirmed by simulations as shown in the supplementary information. All atoms, and therefore also all surface facets, can be recovered in this simulation experiment.

This reconstruction algorithm was applied to the high resolution HAADF-STEM images for both types of Au nanorods. More information on the practical implementation can be found in the methodology section. A visualization of the final result is presented in figures 2a and 2b, where orthogonal slices *through* the 3D reconstruction of the rods synthesized with the CTAB and the Gemini surfactant are presented, respectively.

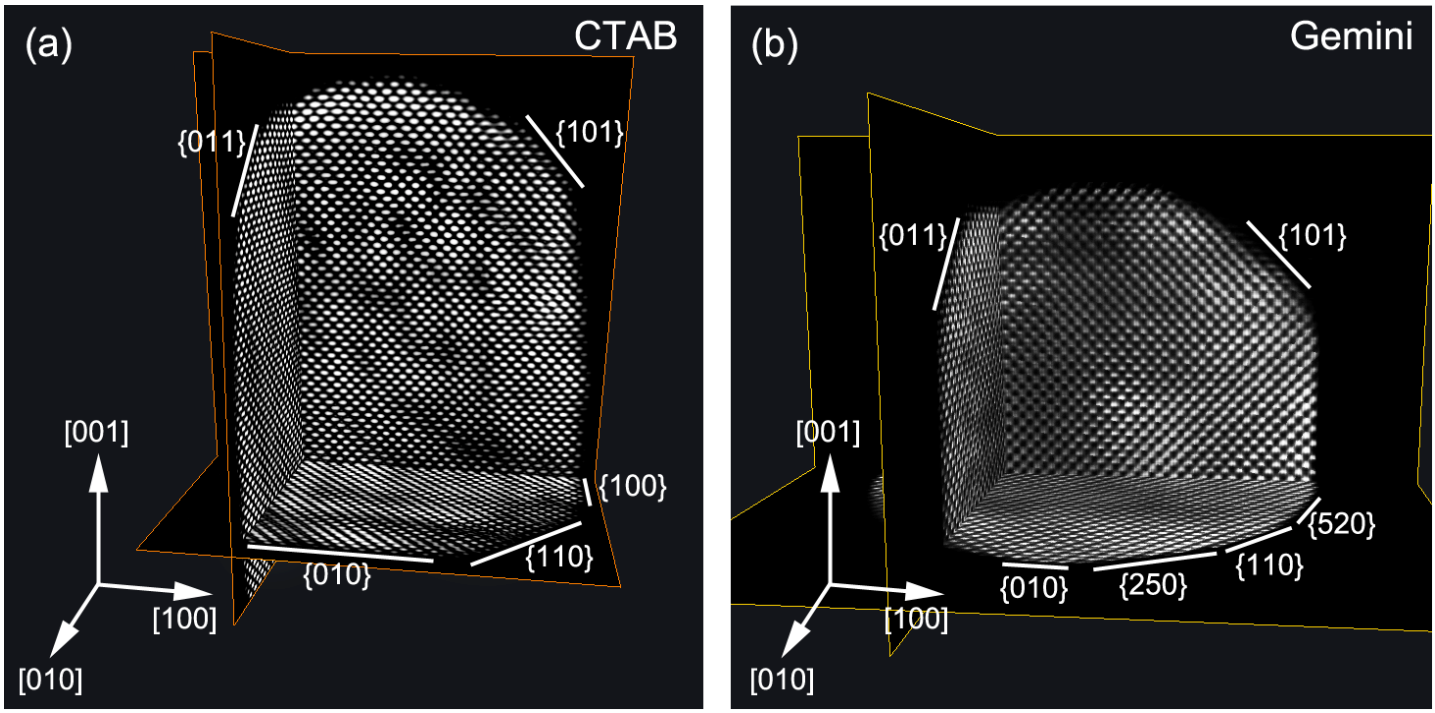

Figure 2: 3D reconstruction of Au nanorods. (a) Three orthogonal slices *through* the reconstruction of a nanorod grown with CTAB, showing individual atom positions. It can be seen that {110} and {100} facets compose the morphology of the rod. The tip is rounded, with clear terraces at the {101} planes. (b) Three corresponding slices through a reconstruction of a nanorod synthesized with the Gemini surfactant. For this rod a more rounded morphology of the cross section is observed including {520} facets. The facets composing the tip of the nanorod are comparable to these of the nanorod grown with CTAB.

From the reconstruction presented in figure 2a, it can be directly concluded that the cross-section of the rod grown with CTAB is bound by alternating {100} and {110} planes, as proposed by Wang et al.[17] . This is in agreement with the HAADF-STEM profiles presented in figure 1. From the 3D reconstruction presented in figure 2b, the facets of the rod grown using the Gemini surfactant can be characterized as {520} planes. These facets were also observed in a previous study by Carbó-Argibay et al.[3] where high resolution TEM was performed on Au nanorods standing perpendicular on the support grid. As can be observed in figure 2, the tip of both nanorods has a rounded morphology with well-defined terraces corresponding to {110} facets.

For the reconstruction obtained for the nanorod grown using CTAB, a 3D Fourier transform was calculated. Projections from this Fourier transform are displayed in figure 3a-c. An animated view of the 3D Fourier transform can be found in the supplementary information. The projections of the Fourier space along the [100], [110] and [111] directions are in good agreement with the theoretical models for a face centered cubic (fcc) crystal lattice, which are illustrated in figures 3d-i. A 3D model of the reciprocal lattice is illustrated in figures 3d-f whereas projections of the reciprocal lattice are presented in figures 3g-i. The correspondence between the model and the experimental Fourier transform of the tomographic reconstruction is remarkable since no prior knowledge about the crystal structure was used during the reconstruction process. The ability to characterize the boundary facets at the atomic scale is of great importance to understand the growth, reactivity, and adsorption properties of these nanorods. In fact, observation of different types of boundary facets for nanorods obtained through slightly different synthetic procedures raises additional questions regarding nanocrystal growth and stability.

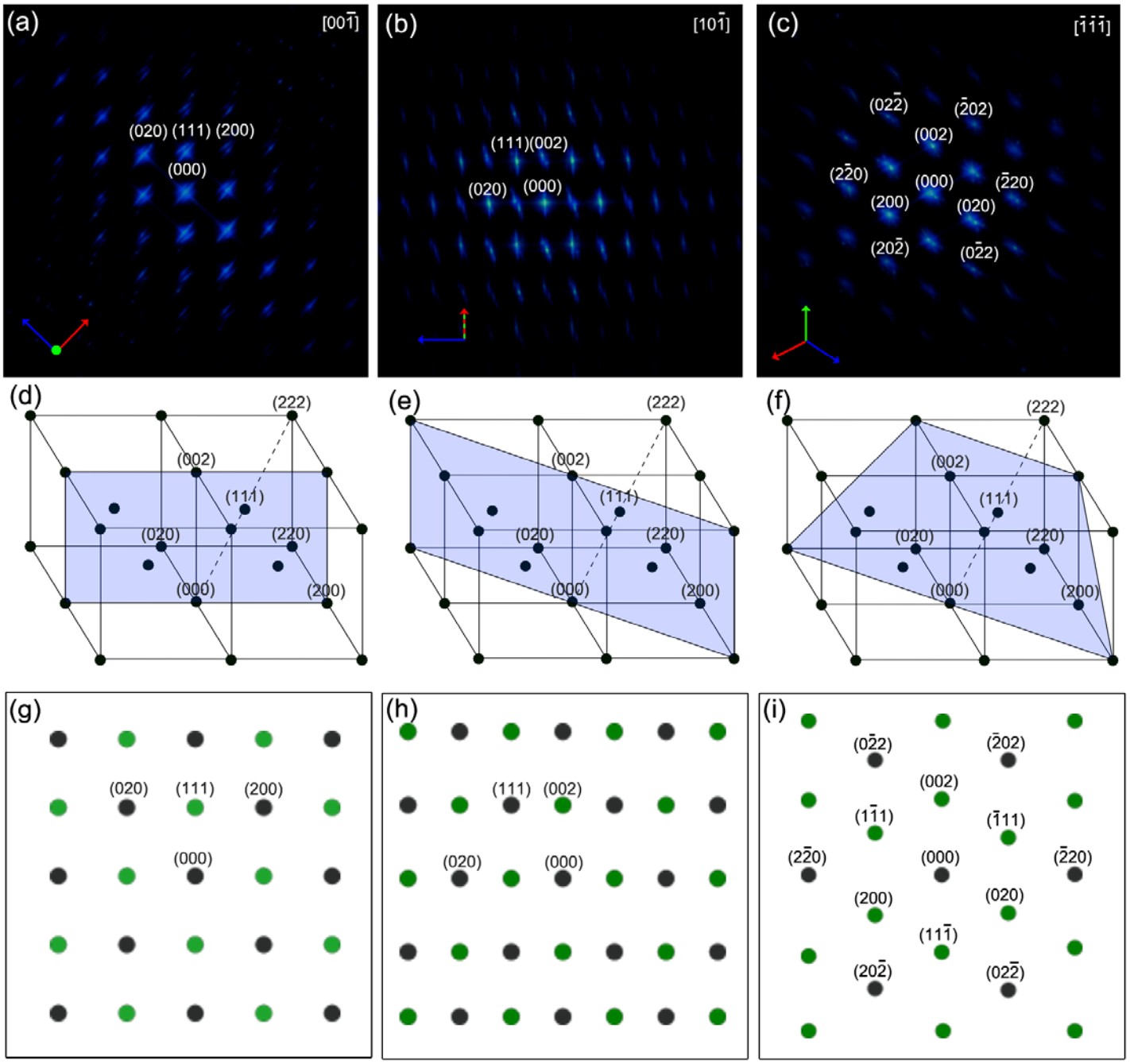

Figure 3: 3D Fourier transform of the reconstructed CTAB nanorod. (a-c) Projections of the calculated 3D Fourier transforms of the reconstructed nanorod obtained along different directions. (d-f) Theoretical model corresponding to the 3D reciprocal space of a face centered cubic (fcc) crystal structure. The plane indicated in blue represents the central plane through the reciprocal space perpendicular to the projection directions of figures (a-c). (g-i) Schematic illustrations of the projections of the Fourier transform along the projection directions of figures (a-c). The grey reflections are present

in the blue layer as indicated in figures (d-f) whereas the green reflections are located above or below this central layer.

While the facets composing the morphology can be clearly recognized in the final reconstructions, also more detailed information at the atomic scale can be extracted from the reconstruction. Figure 4c, corresponding to a more detailed view of figure 4a and 4b, reveals the presence of an atomic surface step with a thickness of two atomic layers. This surface terrace is located at a {001} side facet and it is clear that these steps will have its impact on surface energy and many related nanoscale phenomena, including catalytic, mechanical and electronic properties[27,28].

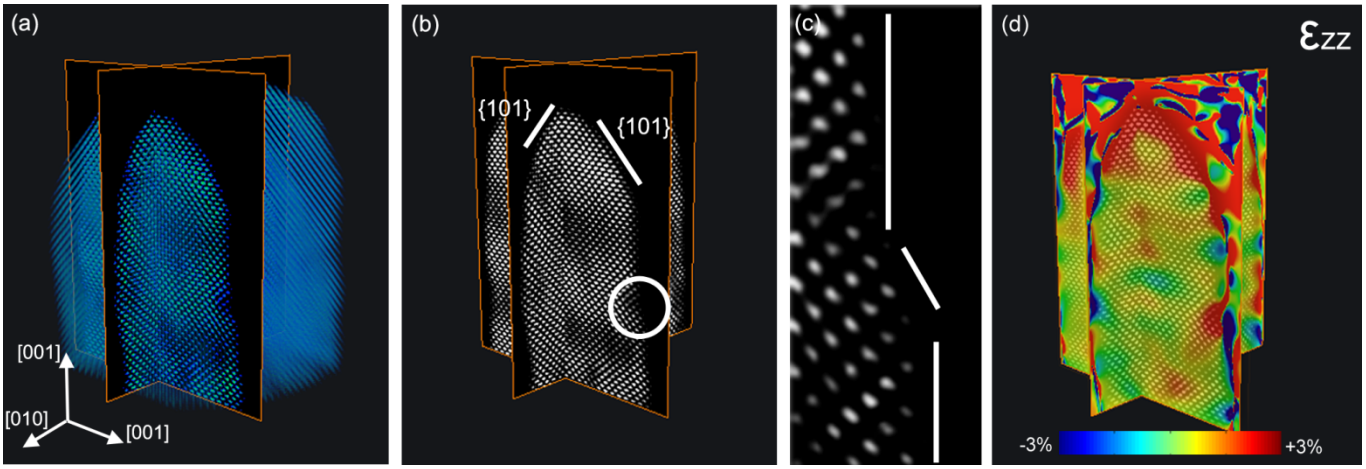

Figure 4: Atomic resolution reconstruction of Au nanorod. (a) Volume rendering of the reconstructed nanorod with two selected slices through the reconstruction. (b) The two slices from figure 4a show that the tip of the nanorod is composed of {101} facets. A region with an atomic surface step is indicated. (c) A more detailed view of the region encircled in figure 4b. In this region, a surface step with a thickness of two atoms is observed in the tomographic reconstruction. (c) Slices through 3D ε_{zz} strain measurement indicating an outward relaxation of the atoms at the tip of the nanorod.

It is important to note that the atom positions are not assumed to be fixed during the reconstruction process. Therefore, the reconstruction presented in figure 2 can serve as a starting point to investigate strain in 3D. Here, we apply the geometrical phase analysis (GPA) to a 3D reconstruction rather than to a 2D projection of a 3D object[29,30]. More details on the approach and its reliability can be found in the methodology section, whereas the

reliability of the approach is discussed, based on simulation experiments, in the supporting information. By selecting three reflections for GPA analysis, we obtain the full 3D ε_{zz}, strain field, which is presented in figure 4d. A reference region where no strain is present, was selected in the middle of the nanorod. This implies that all strain measurements are relative with respect to this reference region. The color code in figure 4d corresponds to the strain in the nanorod and is scaled between -3% (blue) and +3% (red). The error on these measurements is estimated through simulation experiments (as explained in the supplementary information) and equals ±1.3%. It is likely that because of this uncertainty the strain field in the center of the nanorod shows slight deviations from the equilibrium value. The corresponding reconstructed atomic lattice is displayed in figures 4a and 4b. Figure 4a shows a 3D rendering, whereas in figure 4b orthoslices through the reconstruction are presented. This atomic scale 3D reconstruction in combination with the 3D ε_{zz} strain field provides unique information about the relationship between the atomic lattice and the intrinsic strain present in the nanorod. For example, it is clear that the tip of the nanorod is (approximately 3%) positively strained at its end. The measured anisotropy present in the ε_{zz} strain map may be of importance towards understanding the optical properties of the nanorods[1,31] .

In this work, we have characterized the 3D atomic structure of free-standing Au nanorods using a new compressive sensing based reconstruction algorithm. Using high resolution HAADF-STEM projection images and no prior knowledge on the atomic structure, the fcc crystal lattice is reproduced. The side facets of the rods were determined to be either {100} and {110} facets for rods grown with CTAB and {520} facets for the rods synthesized with the Gemini surfactant, which raises an issue regarding the influence of the surfactant on the stability of different facets. At the tip of the nanorod, the morphology of both rods was found to be composed of {101} and {111} facets. Using our approach, 3D strain measurements can be obtained and correlated to the atomic lattice of the nano-object. Although the methodology proposed here is only applied to Au nanorods, it also opens perspectives for the 3D atomic scale visualization of different nanomaterials including single crystals and bimetallic nanocrystals which may lead to a better understanding of their opto-electronic properties.

Methods summary:

Sample preparation:

Au nanorods were synthesized using the well-known seeded growth method [16]. Au nanorods with {520} boundary facets were prepared by overgrowth in the presence of a gemini surfactant, as recently reported[32]. The nanorods were then dispersed in H_2O, deposited on a C grid and plasma cleaned with a H_2/O_2 gas mixture for 15sec.

Low magnification tomography:

A low magnification HAADF-STEM tilt series was acquired in HAADF-STEM mode as described previously. The tilt angles for the CTAB synthesized rod ranged from -75º to +60º with a 5º tilt increment. For the nanorod grown with Gemini, the tilt series ranges between -72º and +74º with an increment of 2º between two successive tilt angles. Alignment of the tilt series was done using a combination of cross correlation methods in FEI Inspect3D and a manual alignment performed in the IMOD software[33]. The reconstruction was performed with a novel total variation minimization reconstruction algorithm to minimize artifacts in the reconstruction[23]. Prior to image acquisition, an electron diffraction pattern was recorded to facilitate indexing of the final reconstructions.

HAADF-STEM imaging:

HAADF-STEM imaging was performed at an aberration corrected cubed FEI Titan 50-80 operated at 300kV. During the tilt experiments, the investigated samples were mounted on a motorized rotation tomography Fischione 2040 holder. This holder can both rotate the sample in plane and tilt the sample over an angular range of ±75º enabling us to reach 4 different major zone axes. The 4 zone axes that are used correspond to the [100], the [110], the [010] and the [$\bar{1}$10] axis. A probe semi convergence angle of 21.4mrad was used during the acquisition. The HAADF detector was mounted at a camera length of 110mm to guarantee incoherent imaging of the Au nanorod. To reduce sample drift during the experiment, the specimen holder was allowed to relax after each tilting step for several minutes prior to image acquisition.

High resolution tomography:

The 3D atomic lattice of the Au nanorods is determined using a novel compressive sensing based reconstruction algorithm where 4 HAADF-STEM projections are used as input. Alignment of the images was done by calculating the center of mass in each projection as proposed by Scott et al[14]. The reconstructions were calculated based on the iterative CS algorithm as explained above. This algorithm was implemented in Matlab using a penalty parameter λ of 0.5. Earlier work and simulation experiments showed that this is a suitable value [23]. In order to minimize remaining fanning artifacts for the reconstruction shown in figure 2b, a convolution in Fourier Space was carried out with the reconstruction shown in figure 1b. More details on the implementation and simulation experiments confirming the validity of this reconstruction technique are provided in the supplementary information.

Geometrical phase analysis:

3D Geometrical phase analysis was implemented in Matlab by selecting three reciprocal lattice points. During the 3D GPA analysis, a Gaussian selection window was used with such a diameter that the spatial resolution of the strain determination equals 1nm.

References

1 Pecharroman, C., Perez-Juste, J., Mata-Osoro, G., Liz-Marzan, L. M. & Mulvaney, P. Redshift of surface plasmon modes of small gold rods due to their atomic roughness and end-cap geometry. *Phys Rev B* **77**, doi:Artn 035418 Doi 10.1103/Physrevb.77.035418 (2008).

2 Chang, L. Y., Barnard, A. S., Gontard, L. C. & Dunin-Borkowski, R. E. Resolving the Structure of Active Sites on Platinum Catalytic Nanoparticles. *Nano Lett* **10**, 3073-3076, doi:Doi 10.1021/Nl101642f (2010).

3 Carbo-Argibay, E. *et al.* The Crystalline Structure of Gold Nanorods Revisited: Evidence for Higher-Index Lateral Facets. *Angewandte Chemie-International Edition* **49**, 9397-9400, doi:DOI 10.1002/anie.201004910 (2010).

4 Katz-Boon, H. *et al.* Three-Dimensional Morphology and Crystallography of Gold Nanorods. *Nano Lett* **11**, 273-278, doi:Doi 10.1021/Nl103726k (2011).

5 Batson, P. E., Dellby, N. & Krivanek, O. L. Sub-angstrom resolution using aberration corrected electron optics (vol 418, pg 617, 2002). *Nature* **419**, 94-94 (2002).

6 Erni, R., Rossell, M. D., Kisielowski, C. & Dahmen, U. Atomic-Resolution Imaging with a Sub-50-pm Electron Probe. *Phys Rev Lett* **102**, doi:Artn 096101 Doi 10.1103/Physrevlett.102.096101 (2009).

7 Valden, M., Lai, X. & Goodman, D. W. Onset of catalytic activity of gold clusters on titania with the appearance of nonmetallic properties. *Science* **281**, 1647-1650 (1998).

8 Grzelczak, M., Perez-Juste, J., Mulvaney, P. & Liz-Marzan, L. M. Shape control in gold nanoparticle synthesis. *Chem Soc Rev* **37**, 1783-1791, doi:Doi 10.1039/B711490g (2008).

9 Midgley, P. A. & Dunin-Borkowski, R. E. Electron tomography and holography in materials science. *Nat Mater* **8**, 271-280, doi:Doi 10.1038/Nmat2406 (2009).

10 Midgley, P. A. & Weyland, M. 3D electron microscopy in the physical sciences: the development of Z-contrast and EFTEM tomography. *Ultramicroscopy* **96**, 413-431, doi:Doi 10.1016/S0304-3991(03)00105-0 (2003).

11 Midgley, P. A., Ward, E. P. W., Hungria, A. B. & Thomas, J. M. Nanotomography in the chemical, biological and materials sciences. *Chem Soc Rev* **36**, 1477-1494, doi:Doi 10.1039/B701569k (2007).
12 Van Aert, S., Batenburg, K. J., Rossell, M. D., Erni, R. & Van Tendeloo, G. Three-dimensional atomic imaging of crystalline nanoparticles. *Nature* **470**, 374-377, doi:Doi 10.1038/Nature09741 (2011).
13 Bals, S. *et al.* Three-Dimensional Atomic Imaging of Colloidal Core-Shell Nanocrystals. *Nano Lett* **11**, 3420-3424, doi:Doi 10.1021/Nl201826e (2011).
14 Scott, M. C. *et al.* Electron tomography at 2.4-angstrom resolution. *Nature* **483**, 444-U491, doi:Doi 10.1038/Nature10934 (2012).
15 Perez-Juste, J., Pastoriza-Santos, I., Liz-Marzan, L. M. & Mulvaney, P. Gold nanorods: Synthesis, characterization and applications. *Coordin Chem Rev* **249**, 1870-1901, doi:DOI 10.1016/j.ccr.2005.01.030 (2005).
16 Nikoobakht, B. & El-Sayed, M. A. Preparation and growth mechanism of gold nanorods (NRs) using seed-mediated growth method. *Chem Mater* **15**, 1957-1962, doi:Doi 10.1021/Cm020732l (2003).
17 Wang, Z. L., Mohamed, M. B., Link, S. & El-Sayed, M. A. Crystallographic facets and shapes of gold nanorods of different aspect ratios. *Surf Sci* **440**, L809-L814 (1999).
18 Hartel, P., Rose, H. & Dinges, C. Conditions and reasons for incoherent imaging in STEM. *Ultramicroscopy* **63**, 93-114 (1996).
19 Krivanek, O. L. *et al.* Atom-by-atom structural and chemical analysis by annular dark-field electron microscopy. *Nature* **464**, 571-574, doi:Doi 10.1038/Nature08879 (2010).
20 Nellist, P. D. & Pennycook, S. J. The principles and interpretation of annular dark-field Z-contrast imaging. *Adv Imag Elect Phys* **113**, 147-203 (2000).
21 Candes, E. J. & Wakin, M. B. An introduction to compressive sampling. *Ieee Signal Proc Mag* **25**, 21-30 (2008).
22 Donoho, D. L. Compressed sensing. *Ieee T Inform Theory* **52**, 1289-1306, doi:Doi 10.1109/Tit.2006.871582 (2006).
23 Goris, B., Van den Broek, W., Batenburg, K. J., Mezerji, H. H. & Bals, S. Electron tomography based on a total variation minimization reconstruction technique. *Ultramicroscopy* **113**, 120-130, doi:DOI 10.1016/j.ultramic.2011.11.004 (2012).
24 Saghi, Z. *et al.* Three-Dimensional Morphology of Iron Oxide Nanoparticles with Reactive Concave Surfaces. A Compressed Sensing-Electron Tomography (CS-ET) Approach. *Nano Lett* **11**, 4666-4673, doi:Doi 10.1021/Nl202253a (2011).
25 Gilbert, P. Iterative methods for the three-dimensional reconstruction of an object from projections. *Journal of theoretical biology* **36**, 105-117 (1972).
26 Kim, S. J., Koh, K., Lustig, M., Boyd, S. & Gorinevsky, D. An Interior-Point Method for Large-Scale l(1)-Regularized Least Squares. *Ieee J-Stsp* **1**, 606-617, doi:Doi 10.1109/Jstsp.2007.910971 (2007).
27 Seo, J. *et al.* Transmission of topological surface states through surface barriers. *Nature* **466**, 343-346, doi:Doi 10.1038/Nature09189 (2010).
28 Alivisatos, A. P. Semiconductor clusters, nanocrystals, and quantum dots. *Science* **271**, 933-937 (1996).
29 Hytch, M. J., Snoeck, E. & Kilaas, R. Quantitative measurement of displacement and strain fields from HREM micrographs. *Ultramicroscopy* **74**, 131-146 (1998).
30 Johnson, C. L. *et al.* Effects of elastic anisotropy on strain distributions in decahedral gold nanoparticles. *Nat Mater* **7**, 120-124, doi:Doi 10.1038/Nmat2083 (2008).
31 Ouyang, G., Zhu, W. G., Sun, C. Q., Zhu, Z. M. & Liao, S. Z. Atomistic origin of lattice strain on stiffness of nanoparticles. *Phys Chem Chem Phys* **12**, 1543-1549, doi:Doi 10.1039/B919982a (2010).
32 Guerrero-Martinez, A., Perez-Juste, J., Carbo-Argibay, E., Tardajos, G. & Liz-Marzan, L. M. Gemini-Surfactant-Directed Self-Assembly of Monodisperse Gold Nanorods into Standing Superlattices. *Angewandte Chemie-International Edition* **48**, 9484-9488, doi:DOI 10.1002/anie.200904118 (2009).
33 Kremer, J. R., Mastronarde, D. N. & McIntosh, J. R. Computer visualization of three-dimensional image data using IMOD. *J Struct Biol* **116**, 71-76 (1996).

Acknowledgement

The work was supported by the Flemish Fund for Scientific Research (FWO Vlaanderen) through a PhD research grant to B. Goris. G. Van Tendeloo acknowledges funding from the European Research Council (ERC Advanced Grant 24691 - COUNTATOMS). L.M.L.-M. acknowledges funding from the European Research Council (ERC Advanced Grant 267867 - PLASMAQUO). The authors appreciate financial support from the

European Union under the Seventh Framework Program (Integrated Infrastructure Initiative N. 262348 European Soft Matter Infrastructure, ESMI). The authors also acknowledge financial support from the Flemish Hercules 3 programme for large infrastructure. We also thank Prof. Rosenauer from IFP, Bremen, for the use of the STEMsim program.

Author contribution

B.G. recorded the experimental images. B.G. and W.V.d.B. developed the reconstruction algorithm. B.G. and S.B. further analyzed the 3D reconstructions. E.C.-A. , S.G.-G. and L.L.M carried out particles synthesis and interpreted the results. G.V.T. advised on the methodology, the interpretation and on the paper. All the authors read and commented on the paper.